PHYSICAL REVIEW B VOLUME 45, NUMBER 8 15 FEBRUARY 1992-II

Surface- and interface-plasmon modes on small semiconducting spheres

D. Ugarte,* C. Colliex, and P. Trebbia
Laboratoire de Physique des Solides, Université Paris XI, Bâtiment 510, 91405 Orsay, France

(Received 18 July 1991)

The study of the electronic properties of small particles is of major interest because of their intriguing physicochemical properties. The very small electron probes available in scanning transmission electron microscopes offer unique capabilities for investigating small particles with subnanometer spatial resolution. The correlation between electron-energy-loss spectra and energy-filtered images is of great help in pinpointing the excitations under study. This paper presents a theoretical and experimental study of collective excitation modes in the bulk and at the interfaces and surfaces of small spherical silicon particles covered with a thin oxide coating. Among other results, our experimental measurements have shown that there exists a surface-mode excitation at 3–4 eV, precisely localized on the external surface of the oxide layer. Classical dielectric theory is used in interpreting these results, by invoking the presence of an ultrathin conductive layer.

I. INTRODUCTION

Electronic properties of small objects or microclusters have been extensively studied in recent years. Such media with very small dimensions exhibit chemical and physical behavior substantially different from those of bulk materials. Moreover, the understanding of the small-particle electron affinity is very important because of their wide application in catalysis work.

Analytical electron microscopy constitutes a useful tool to provide locally the electronic properties of small volumes, through various available spectroscopies (EDX, EELS, Auger, secondary electrons, etc.). Among them, electron energy loss spectroscopy (EELS) experiments are well adapted to investigate various electron-excitation modes and particularly the collective ones (plasmons), which are modified in a medium of finite size. The valence loss region yields strong signal levels, and allows access to some electronic-structure properties through a macroscopically defined parameter, the dielectric permittivity, because the phenomena involved are complex and include important many-body effects.[1]

Early theoretical and experimental work[2,3] has dealt with the broad electron-beam geometries ($\sim\mu m^2$) in which a great number of particles are simultaneously analyzed. This configuration presents several experimental difficulties: For example, one must produce samples made of regularly spaced particles, sufficiently diluted to be described as isolated, but dense enough to provide a strong signal. Furthermore, the particles must be of similar shape, with a narrow size distribution, and with as thin an oxide coating as possible. These ideal characteristics are very difficult to attain in practice.

The scanning transmission electron microscope (STEM), which provides a focused 100-kV electron beam within a probe of diameter less than 0.8 nm, allows the study of individual particles with a high degree of spatial resolution. It is possible to introduce the concept of impact parameter, which corresponds to the distance between the primary electron trajectory and some well-defined feature of the investigated particle (center, external surface, etc.). The STEM offers two possibilities to gather information: (i) in the fixed-probe mode, one measures the EELS spectrum for a point in the sample; (ii) in energy-filtered images, one records the number of electrons that have suffered an energy loss corresponding to a particular excitation as a function of the probe position. Consequently, it is possible to measure the energy of various modes as well as their special localization.

Most theoretical work related to STEM measurements has been devoted to the excitation of plasmons in spherical particles. More complex geometries related to the spherical case have been analyzed by Baston[4] for two neighboring spheres, by Wang and Cowley[5] and by Ouyang and Isaacson[6] for a particle interacting with the substrate. Spheroidal targets have also been considered.[7] On the other hand, several authors have reported the possibility of drilling holes of nanometer-size diameter in beam-sensitive materials:[8,9] it has restimulated the interest in energy-loss studies in cylindrical geometry.[10–13]

Up to now, STEM experimental measurements have mostly dealt with metals, and the data interpretation has usually involved modeling the dielectric constants by the Drude expression for a free-electron gas.[14–16] This description is valid for metals with a well-known free-electron response (Al, Ag, Na, etc.), and the inclusion of real damping can provide a realistic description allowing a comparison to be made with experimental data.

The aim of this work is to test the validity of classical dielectric theory for a more general case. We will be concerned with the electronic properties of spherical semiconductor particles, particularly silicon spheres. This material and its oxides have been extensively studied, and are very well characterized, because of their applications in microelectronics. The dielectric properties have been experimentally measured; they present complex structures[17] and provide a stringent test for the theoretical tools that have been developed for the calculation of collective modes in dielectric spheres with arbitrary dielectric response function.

In the present paper, we investigate, under specific STEM illumination angular conditions, the electron-energy-loss spectrum at low energies (1–40 eV) for spherical silicon particles, and the spatial localization of the most important spectral features observed. The results will be compared to predictions of classical dielectric theory.

II. MATERIALS AND METHODS

The experimental work has been performed with a dedicated STEM VG HB501 (for a complete description of the operating conditions, see Mory[18]). The field emission electron gun delivers a 100-kV primary beam of a few 10^{-10} A to the surface of the specimen within a probe 0.5–0.8 nm in diameter, when an optimum angle for focusing (≈ 7.5 mrad) is used. For EELS studies, the microscope is fitted with a magnetic spectrometer Gatan 607 in the serial acquisition mode. Generally a collection aperture of 6.5-mrad semiangle limits the acceptance of the spectrometer. When carefully focused, the spectrometer designed to cancel second-order aberrations, provides a typical sub-electron-volt energy resolution. It implies a full width at half maximum (FWHM) of the order or better than 0.5 eV. However, in the high-energy tail of the elastic peak, a noticeable contribution remains for losses as great as 3–4 eV. When studying EELS features in this low-loss range, one is more concerned with the signal level superposed over the elastic peak background than with the energy resolution. If a 1-eV energy resolution can be currently achieved for spectrum acquisition, closing the selection slit at this level constitutes a more stringent condition for energy-filtered image recording when the dwell time per picture element is limited.

Small semiconducting particles have been prepared by a gas evaporation method using an arc discharge between two electrodes of silicon.[19] The particles are deposited on a holey carbon film, and they have a tendency to coagulate when collected for electron-microscopy observation. Observations have only been performed on those particles hanging over a hole, in order to eliminate the carbon contribution to the spectra.

Figure 1 shows a low-magnification electron micrograph of a group of silicon particles. They are nearly spherical in shape, but show a slight faceting when observed with a high-resolution microscope (HREM). Their size ranges from 10 to 300 nm in diameter, and they are covered by a thin (2–6 nm) natural amorphous oxide layer, produced by exposure to atmosphere during the sample preparation for electron-microscopy observation. Some particles show dark contrast lines running across them close to the center; these lines are due to planar faults, such as twins, produced during their growth.

III. EXPERIMENTAL RESULTS

Typical EELS spectra in the low-energy-loss region are shown in Fig. 2. Spectrum (a) has been acquired in an image mode, with the probe scanning all over a particle of diameter ≈ 50 nm. Spectrum (b) has been acquired in a fixed-probe mode, with the probe located outside the particle at about 2 nm from the external surface (grazing incidence); in this configuration it is possible to measure surface losses without the strong contribution from the volume plasmon, which is present in the case of penetrating trajectories.[20]

Energy-filtered images corresponding to the main spectral features observed have been obtained (Fig. 3) in order to visualize their spatial distribution, as for example the difference between surface and volume excitations. In contrast with inner-shell losses, there is no simple method in the low-loss region for processing an energy-filtered image in order to isolate a desired signal. Consequently,

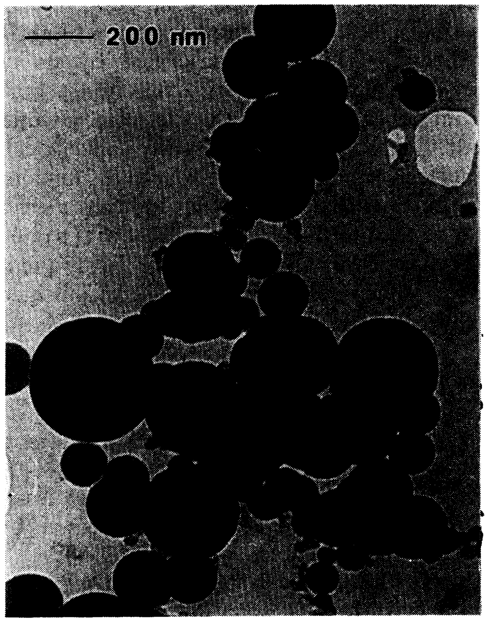

FIG. 1. Conventional electron micrograph of a group of silicon particles.

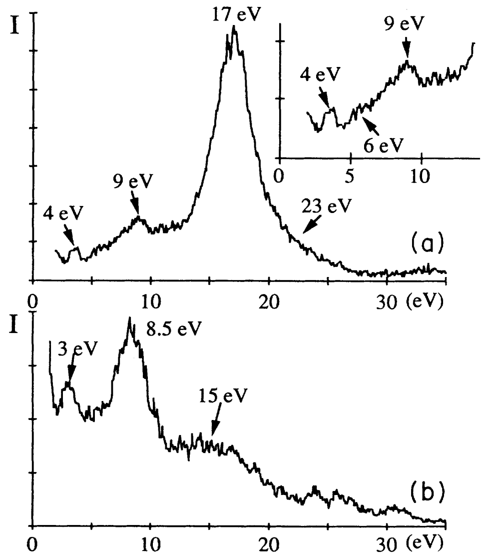

FIG. 2. Typical low-energy-loss spectra of silicon particles: (a) over a particle; (b) grazing incidence.

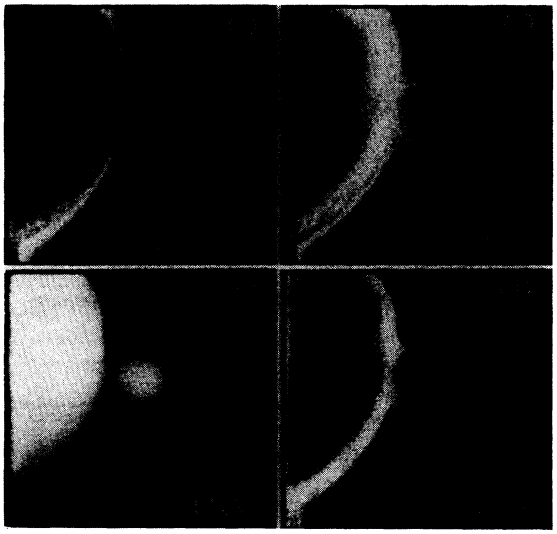

FIG. 3. Series of energy-filtered images of a small silicon particle close to a bigger one.

we are constrained to work with the original images. For a more accurate comparison of the localization of the different excitations, line profile intensities have been extracted from the images along a given direction (see Fig. 4).

On the basis of our previous knowledge of Si-SiO_2 plane interfaces,[21,22] it is possible to draw, from the above observations, the following immediate conclusions.

(i) The 17-eV peak is due to the Si bulk plasmon.[23] In Fig. 3(c), corresponding to this energy loss, the image intensity is maximum in the crystalline core at the center of the particle. As expected, it is not present in the spectrum recorded in grazing incidence [Fig. 2(b)]; the volume plasmon field is therefore zero outside the particle.[20]

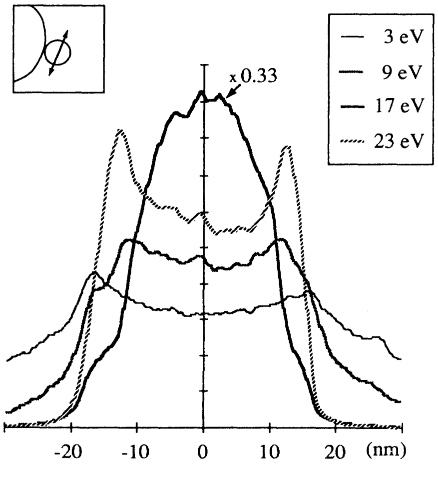

FIG. 4. Line profile intensities extracted from the images in Fig. 3.

(ii) The 23-eV peak is due to the SiO_2 bulk plasmon. It can be seen, in Fig. 3(d), that it is mostly generated within the oxide layer covering the particle.

(iii) The 9-eV contribution is due to the normal surface plasmon of the Si particle. We expect that the energy of this surface plasmon will be found at an energy lower than that of an isolated Si sphere in vacuum [for the dipole mode ($l=1$), $\omega_s = \omega_p/\sqrt{3} = 9.8$ eV], because the effect of a thin oxide layer is to reduce the surface-plasmon frequencies, leading to values dependent on the oxide thickness.[24,25] As expected, it is mainly excited at the interface between the Si core and the Si-oxide layer [Fig. 3(b)], which is predicted by the semiclassical calculations for Al-oxide-covered particles.[24]

(iv) The minor feature at 5.5–6 eV is due to a Si interband transition, and may also contain a carbon contribution to the energy loss, if a small degree of contamination is present.

(v) The minor features at 10.5 and 12 eV are due to SiO_2 interband transitions.[17]

(vi) Finally the low-energy peak at 3–4 eV is an unexpected result, since a careful look at Fig. 3(a) shows that the radius of this image is greater than that of the 9-eV one. This means that this mode is not excited at the Si-SiO_2 interface, but on the external surface (SiO_2 vacuum interface) of the oxide layer.

IV. DISCUSSION

A. Classical dielectric theory: A summary

Several approaches[20,24–27] can be used to calculate the plasmon frequencies and their excitation probabilities in spherical particles. Among them, Ferrell and Echenique[28] have presented a formalism using classical dielectric theory, which is valid for any arbitrary dielectric function $\epsilon(\omega)$. It yields the total energy loss suffered by a classical point charge moving in a straight-line trajectory through a medium described by its complex, frequency-dependent, dielectric function $\epsilon(\omega,\mathbf{q})$, the momentum dependence $\mathbf{q}$ of the dielectric permittivity is neglected. This assumption is usually called local theory, because it does not consider the spatial dispersion or nonlocal effects; thus the polarization induced at each point is directly related to the electric field at that same point.

The validity of this approach is limited by the fact that if the object becomes very small, quantum-mechanical effects may be important and the macroscopic-dielectric-function formulation is no longer a valid description of the electronic structure. This "quantum size effect" produces a blue shift in the oscillation frequency.[16,25,26,29,30] This energy shift may be neglected for particles of radius greater than 8 nm.[15,16,26]

On the other hand, for particles of radius less than 20 nm, retardation effects can also be neglected.[31] Consequently, for those particles with radius $8<R<20$ nm, one can solve the classical static dielectric problem, instead of the full Maxwell equations, in order to calculate the electric field $\mathbf{E}$ of the system.

The Laplace equation to be solved is

$$\nabla^2\Phi=0 \, , \tag{1a}$$

with

$$\mathbf{E}=-\nabla\Phi \, . \tag{1b}$$

The usual boundary conditions are imposed upon the solutions of these equations: continuity of the parallel electric field and of the normal electric displacement field components.

The resulting equations have nontrivial solutions only for certain frequencies, given implicitly by the energy dependence of the dielectric functions of the different components in the analyzed system. These frequencies are the surface-plasmon modes.

The total energy loss W can be calculated by solving Poisson's equation to obtain the electric field:

$$\nabla^2\Phi=-4\pi\rho \, , \tag{2a}$$

with

$$\mathbf{E}=-\nabla\Phi \, , \tag{2b}$$

where ρ is the charge density and Φ the electrostatic potential.

The electron may then be represented by a time-dependent charge density:

$$\rho=-e\delta(x)\delta(y-d)\delta(z-vt) \, , \tag{3}$$

where v is the electron velocity and d is the impact parameter related to some specimen feature (see Fig. 5 for the case of an oxidized sphere).

For an electron traveling from $z=-\infty$ to $+\infty$, the work W done by the induced field on the impinging electron is

$$W(d)=-e\int_{-\infty}^{+\infty}\mathbf{E}_i\cdot d\mathbf{z} \, . \tag{4}$$

This expression can be compared to the total energy loss calculated as a sum over all energy losses with their probability of occurrence $P_\omega(d)$ at an impact parameter d:

$$W(d)=\int_0^{+\infty}\hbar\omega P_\omega(d)d\omega \, . \tag{5}$$

Using a quantum-mechanical treatment, Ritchie and Howie[32] have established that this approximation is valid, provided that all inelastic electrons are collected, and that the calculated probability is convoluted with the spatial distribution of electrons in the probe. Howie and Milne,[21] and Walls and Howie,[22] have applied this theory to interpret EELS results for the case of a plane interface between silicon and silicon oxide.

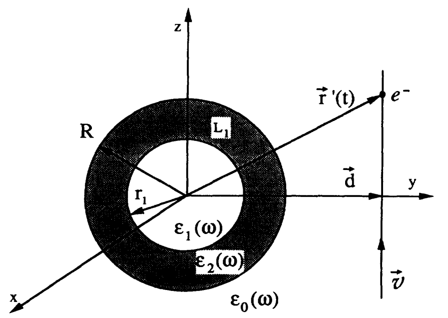

FIG. 5. Electron traveling with a velocity v at an impact parameter d from an oxidized sphere of external radius R.

For spherical coordinates, Ferrell and Echenique[28] have deduced from this formalism an analytical expression, including all multipolar contributions, for the energy loss suffered by an electron traveling outside the particle. This derivation was then extended to take into account the presence of an oxide coating[33] and the case of penetrating trajectories.[34]

B. Comparison of the experimental results with the predictions of the classical theory

Figure 6 shows the results of the calculation of the energy-loss probability for an electron traveling outside an oxidized silicon particle.[33] The lower part of the figure presents the contributions of selected individual multipoles, and in the upper part the results of the partial additions up to $l_{\max}=15$. A crystalline Si sphere, covered with an amorphous SiO_2 layer, has been considered, with dimensions similar to the small particle shown in Fig. 3. The experimental dielectric coefficient introduced in the calculation was taken from Palik.[17] Many multipoles ($l\leq 15$) have been included to obtain a stable result.

The energy of the surface plasmon peak is about 9 eV, but it changes in intensity and energy with l. The predicted energy agrees well with the measured one, but the narrow shape of the peak is different from the experimental one. Walls and Howie[22] have tried to overcome this

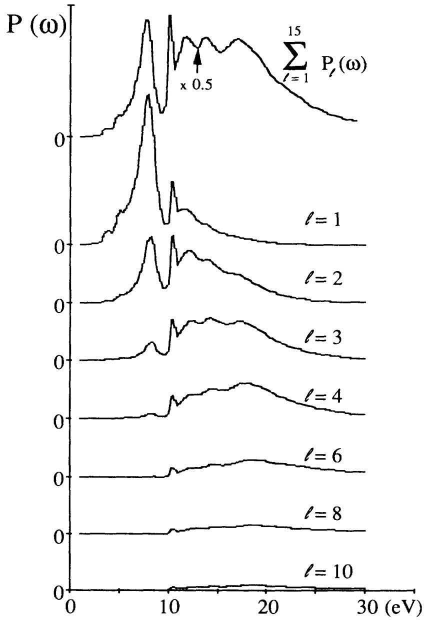

FIG. 6. Energy-loss probabilities for the case of a silicon core covered with a SiO_2 (glass) surface layer ($R=17.1$ nm; $r_1=11.6$ nm; $d=17.6$ nm).

discrepancy by including a thin layer of monoxide of silicon at the interface between Si and SiO_2 to improve the modeling of a gradual reduction of the oxygen content across the interface, but the agreement with experiment remains poor.

Energy losses due to oxide covering are only present for energies greater than the band gap of SiO_2, i.e., 8.9 eV. Two major peaks, associated with interband transitions at 10.5 and 12 eV are predicted. Beyond these peaks the intensity decreases with some slight oscillations.

The surface-plasmon intensity is negligible for $l>4$, and higher-order multipoles mainly exhibit contributions generated in the oxide layer. It has already been reported that oxide coatings reduce the contribution of high-order multipoles[25,35] to the surface plasmon, and that these high-order modes are dominated by the oxide losses.[35]

Two weak steps are visible at 3.4 and 5.6 eV. They correspond to interband transitions in silicon, and are also visible in the energy-loss function $[\mathrm{Im}(-1/\epsilon)]$ for this material. They are related to volume properties of silicon, and cannot be associated with the experimental peak at 3–4 eV, with an obvious surface character in the energy filtered image.

C. Possible interpretations for the 3–4-eV surface loss

Batson[14] has also recorded an unexpected peak at 3–4 eV in a similar experiment on oxidized Al spheres. This low-loss peak was only present for a small sphere lying on a larger one and has never been observed for isolated Al particles. This phenomenon has been interpreted as the result of a coupling of the surface plasmons at the point of contact between two neighboring particles, where a narrow metal-oxide-metal interface exists.[4] In our work, the spatial localization of the low-energy excitation does not exhibit the dipole distribution around the point of contact of the spheres, as was observed by Batson; moreover, it can be seen in all particles. This difference is very important, and constitutes a clear argument for analyzing the problem with an isolated particle model.

Furthermore, in this energy range the complex part of the dielectric permittivity for crystalline silicon reaches high values $[\epsilon_2(3.4\text{–}4.0\text{ eV})>30]$, so that any oscillation would be heavily damped. Because the real part of $\epsilon(\omega)$ also exhibits high values $[\epsilon_1(2.8\text{–}3.5\text{ eV})>20]$, the existence of Cerenkov radiation could be suggested. Its contribution, however, remains negligible for the relatively large collection angles (several mrad) currently used in the scanning transmission electron microscope.

If we assume that the natural surrounding oxide layer is made of amorphous SiO_2 (i.e., an insulator with a band gap of 8.9 eV), the localization of the 3–4 eV loss process on the external surface (SiO_2-vacuum) of the oxide layer constitutes an anomalous phenomenon. It is well known that insulators cannot absorb at energy values in the gap ($\epsilon_2\equiv 0$), nor can they sustain surface plasmons in this energy range. It suggests the existence of some kind of induced surface phenomena (charge, contamination, radiation damage, etc.).

As for the influence of a contamination layer of amorphous carbon, no important effect can be observed in the low-loss range. This fact can easily be understood by considering the surface plasmon at a plane interface between two materials a and b. The condition for resonance is $\epsilon_{1a}(\omega)+\epsilon_{1b}(\omega)=0$.[36] Consequently, if medium a is SiO_2 $[\epsilon_1(0\text{–}7\text{ eV})\approx 2.2]$, an interface plasmon in the 3–4-eV region would require the medium b to be a conductor, or at least a semiconductor with negative values $[\epsilon_{1b}(3\text{–}4\text{ eV})<0]$ for the dielectric permittivity. Although the conditions for resonance in a spherical geometry are more complex, this consideration still holds. The real part of the dielectric function of amorphous-C (Ref. 37) is positive in the low-energy region $[\epsilon_1(1\text{–}19)\text{eV})>0]$, so an amorphous carbon layer on the coated silicon particle cannot induce a new collective surface oscillation in this energy range.

The effect of oxygen desorption, induced by electron irradiation, on oxide surfaces is a well-known phenomenon in electron microscopy. STEM analysis usually requires very high electron doses to get a good signal-to-noise ratio. In the present work, for example, doses as high as $10^8 e^-/\mathrm{nm}^2$ have been necessary in recording the series of micrographs in Fig. 3. Under the assumption that the SiO_2 surface is damaged by the beam and loses some oxygen, a thin conducting film could be produced on the surface.[38] We have therefore been led to study the surface oscillations generated by a thin conducting spherical shell.

D. General properties of surface excitations in a conducting spherical shell

A conducting surface coverage sustains two surface plasmons,[35] one, ω_s, at the external surface and a second one, ω_v, at the internal surface, like that of a void. To visualize clearly this phenomenon, Fig. 7(b) compares the energy-loss probability for a thin metallic shell with that of a solid metallic sphere. The surface plasmon of the particle splits into two modes. For the sake of simplicity, the Drude model of the dielectric permittivity for aluminum ($\omega_p=15$ eV) has been used.

Figure 7(a) displays the frequencies of the surface modes as a function of the relative thickness of the metallic shell (R/r_1), calculated using the quasistatic approximation introduced above. Considering the different limit situations in Fig. 7(b), for a thick metallic ($R/r_1\to\infty$) shell, we obtain the two frequencies of a void in a infinite matrix:

$$\omega_{\text{void}}=\left[\frac{l+1}{2l+1}\right]^{1/2}\omega_p\ , \tag{6}$$

and that of a isolated aluminum sphere,

$$\omega_s=\left[\frac{l}{2l+1}\right]^{1/2}\omega_p\ . \tag{7}$$

If the shell becomes thinner ($R/r_1\to 1$) the surface plasmons of both interfaces interact and a strong coupling is observable, producing a shift of the resonant frequencies. In this case the association of a mode with an

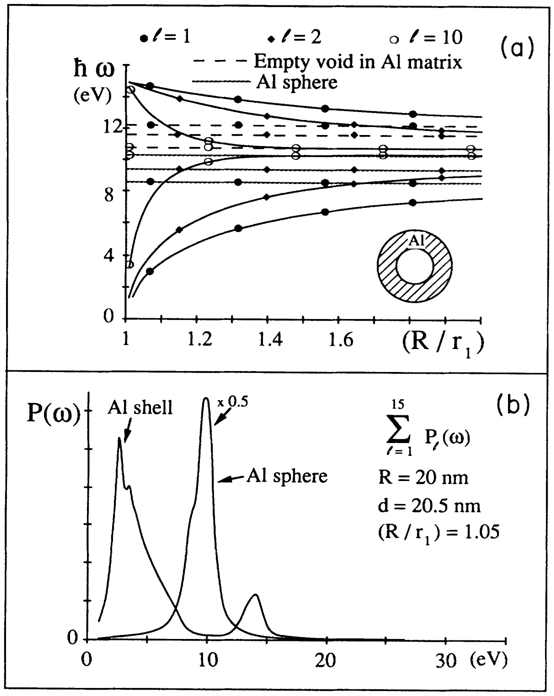

FIG. 7. Properties of collective surface modes of a thin metallic spherical shell. (a) Eigenfrequencies as a function of the relative radius of the external and internal surfaces R/r_1; (b) energy-loss probability for the case of a grazing-incidence electron.

interface is not possible, because they are the result of the oscillations of the electrons of the whole system. This phenomenon has been known for a long time in the case of a plane geometry (Ritchie[39]). If the thickness of the film becomes small enough, the two surface excitations are coupled. Thus two new frequencies are created, ω^- and ω^+; and the ω^- mode reduces its energy with decreasing film thickness.

The low-energy peak observed in the present study could therefore be interpreted as the ω^- branch of the coupled surface excitation on a thin conducting surface layer covering the particle. Furthermore it would explain its localization on the outermost surface of the sphere. The existence of the thin metallic coating creates an extremely inhomogeneous system, with a highly heterogeneous electric field, for which the influence of high-order multipoles should be increased. The strong contribution of the high l values for the ω^- mode, may explain the sharp contrast induced in the energy filtered image[40] [Fig. 3(a)].

E. Detailed calculations for the double-coated sphere

In the framework of the classical dielectric theory, the coated-particle model (Fig. 5) is now extended to include the effect of a second coating layer L_2 (Fig. 8).

The frequencies of the surface-plasmon modes are determined by the solutions of the equation

$$0=-(\alpha\gamma)^{2l+1}a_{03}a_{32}a_{21}-\alpha^{2l+1}d_{03}d_{32}a_{21}l(l+1)$$
$$-\gamma^{2l+1}l(l+1)a_{02}d_{32}d_{21}-l(l+1)d_{03}a_{23}d_{21}\ , \quad (8)$$

where

$$a_{ij}=\epsilon_i(l+1)+\epsilon_j l,\quad d_{ij}=\epsilon_i-\epsilon_j$$

and

$$\alpha=\frac{r_2}{r_1},\quad \gamma=\frac{R}{r_2}\ .$$

We have solved the equation in order to calculate the energy-loss probability for the general case of both external and internal trajectories, i.e., whether or not the electron penetrates the particle. The total contribution of each multipole is, as in[41]

$$P_l(\omega,d)=\sum_m P_{lm}(\omega,d)\ , \quad (9)$$

where

$$P_{lm}(\omega,d)=\text{const}\times(2-\delta_{0m})\frac{(l-m)!}{(l+m)!}(\tilde{\chi}^{1}_{l_m}r_1^{-l}f_{11}+\tilde{\chi}^{2}_{l_m}r_1^{-l}f_{21}+\tilde{\chi}^{3}_{l_m}r_2^{l+1}f_{22}+\tilde{\chi}^{4}_{l_m}r_2^{-l}f_{31}$$
$$+\tilde{\chi}^{5}_{l_m}R^{l+1}f_{32}+\tilde{\chi}^{6}_{l_m}R^{l+1}f_{42})\ , \quad (10)$$

where

$$f_{1h}=2\int_0^{(r_1^2-d^2)^{1/2}}P_l^m[z/(d^2+z^2)^{1/2}]S_{lh}(r')\xi_{l-m}(z)\frac{dz}{v}\ , \quad (11a)$$

$$f_{2h}=2\int_{(r_1^2-d^2)^{1/2}}^{(r_2^2-d^2)^{1/2}}P_l^m[z/(d^2+z^2)^{1/2}]S_{lh}(r')\xi_{l-m}(z)\frac{dz}{v}\ , \quad (11b)$$

$$f_{3h}=2\int_{(r_2^2-d^2)^{1/2}}^{(R^2-d^2)^{1/2}}P_l^m[z/(d^2+z^2)^{1/2}]S_{lh}(r')\xi_{l-m}(z)\frac{dz}{v}\ , \quad (11c)$$

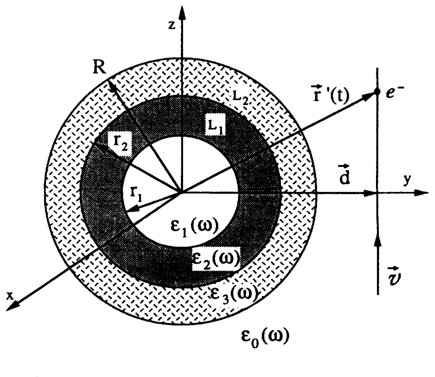

FIG. 8. Electron traveling with a velocity v at an impact parameter d from a doubly coated sphere of external radius R.

$$f_{4h}=2\int_{(R^2-d^2)^{1/2}}^{+\infty}P_l^m[z/(d^2+z^2)^{1/2}]S_{lh}(r')\xi_{l-m}(z)\frac{dz}{v}\ , \tag{11d}$$

where $P_l^m(x)$ is a generalized Legendre polynomial, and

$$r'=(d^2+z^2)^{1/2}\ ,$$

$$S_{lh}(r')=\begin{cases}(r')^l & \text{for } h=1\\ (r')^{-(l+1)} & \text{for } h=2\ ,\end{cases}$$

$$\xi_{l-m}(z)=\begin{cases}\cos(k_z z), & l-m \text{ odd}\\ i\sin(k_z z), & l-m \text{ even}\ ,\end{cases}$$

and

$$\begin{aligned}\tilde{\chi}_{lm}^k=&\,x_l^{k,1}[(f'_{42}+f'_{32}+f'_{22})r_1^l+f'_{11}r_1^{-(l+1)}]\\ &+x_l^{k,2}[(f'_{42}+f'_{32})r_2^l+(f'_{21}+f'_{11})r_2^{-(l+1)}]\\ &+x_l^{k,3}[f'_{42}R^l+(f'_{31}+f'_{21}+f'_{11})R^{-(l+1)}],\end{aligned} \tag{12}$$

where $f'_{1h}=f_{1h}$ but with $\xi_{l-m}(z)$ replaced by

$$\xi'_{l-m}(z)=\begin{cases}\cos(k_z z), & l-m \text{ odd}\\ -i\sin(k_z z), & l-m \text{ even}\ .\end{cases}$$

A brief outline of the calculation is given in the Appendix, as well as the analytical expression of the coefficients $x_l^{k,n}$.

This expression accounts for the surface losses only, and in the case of penetrating trajectories, we must add the volume plasmon contribution $P_v^i(\omega)$, of each constituent material i, to the total energy loss:

$$P_T(\omega,d)=\sum_l P_l(\omega,d)+\sum_i P_v^i(\omega,d)\ . \tag{13}$$

Usually, this formula includes a third term, the Begrenzungeffekt,[42] that accounts for the reduction of the volume loss probability due to the surface excitations.[14,39] In our case this extra term is implicitly included in the first one: for penetrating trajectories, the surface loss probability become negative for energies below the volume plasmon beak. Within the thin-film approximation, the volume loss probability can be written as[43]

$$P_v^i(\omega,d)=\frac{te^2}{\pi^2\hbar v^2}\text{Im}(-1/\epsilon)\ln[1+(\beta/\theta_E)^2]\ , \tag{14}$$

where t is the path of the electron inside the material i, β is the collection angle, and θ_E is the characteristic angle of inelastic scattering, associated with an energy loss $\hbar\omega$($\theta_E=\hbar\omega/pv$; p is the momentum of the electron).

If we consider the case of an external electron, the expression is simplified, and yields an analytical result, as published by Echenique, Howie, and Wheatley:[33]

$$P_l(\omega,d)=\frac{e^2R}{\pi^2\epsilon_0\hbar v^2}\sum_{m=0}^{l}\left[\frac{(2-\delta_{0m})}{(l-m)!(l+m)!}\right]\text{Im}(-\sigma_l)\times(\omega R/v)^{2l}K_m^2(\omega d/v)\ , \tag{15}$$

where

$$\sigma_l=[x_l^{6,1}(\alpha\gamma)^{-l}+x_l^{6,2}\gamma^{-l}+x_l^{6,3}]\ . \tag{16}$$

$K_m(x)$ is a modified Bessel function of order m,

The expressions for σ_l for the oxide-free particle, or for the oxidized particle,[30] can be obtained taking the correct limits of expression (16) and choosing the dielectric permittivities $\epsilon_j(\omega)$ for the different constitutive materials.

F. Comparison of the predictions of the theory for a three-shell model with the experimental results

In order to model the conducting layer, we have assumed an amorphous layer of silicon at the surface, as a result of oxygen desorption from the SiO_2 surface. This assumption does not imply that a completely oxygen-free layer exists, but it constitutes a logical model for the conductive layer induced by electron bombardment of the SiO_2 surface. The thickness of this layer has been chosen as 0.5 nm for the calculation, in order to represent a film thinner than the diameter of the probe. This thickness cannot be detected by other STEM imaging techniques, but should be sufficiently thick for a description, to a first approximation, by its macroscopic dielectric response.

The calculation using the experimental parameters from Fig. 3 for the particle radius and the Si core, together with a 0.5-nm amorphous Si surface layer, is shown in Fig. 9. As before, we show independent multipole contributions in the lower part of the figure, and a partial addition in the upper part. The thin (semi)conducting film induces dramatic effects; the theoretical results now contain an important contribution in the low-energy range (4–5 eV), while the normal surface mode at 9 eV is not modified.

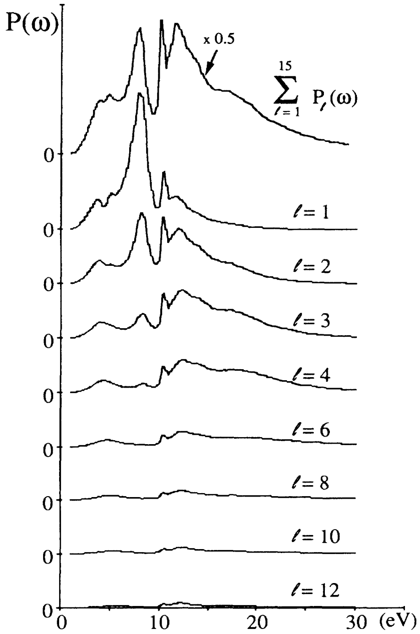

FIG. 9. Energy-loss probabilities for an electron traveling outside of a doubly coated silicon core, covered with a SiO_2 (glass) and an amorphous silicon (a-Si) surface layer ($R=17.1$ nm; $r_1=11.6$ nm; $r_2=16.6$ nm; $d=17.6$ nm).

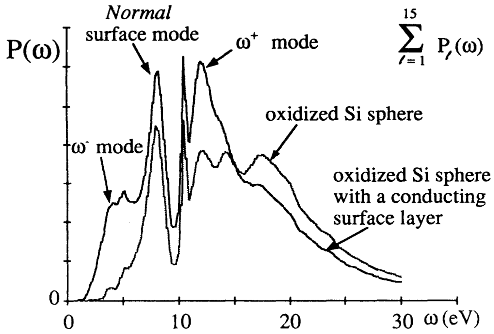

FIG. 10. Energy-loss probabilities. Comparison between the simple oxidized and the doubly coated silicon sphere ($R = 17.1$ nm; $r_1 = 11.6$ nm; $r_2 = 16.6$ nm; $d = 17.6$ nm).

The normal surface plasmon at 9 eV is correctly described using only the first four multipoles. For the surface plasmon at low energy, higher modes make important contributions even for values of $l \sim 10$, showing that many l values must be included to account for the thin conducting film covering the particle. This high-l-value contribution induces a narrower localization of this excitation.[40]

In Fig. 10, the loss probabilities for the double-coated silicon sphere and the simple oxidized case are compared, showing that two additional oscillations ω^-, ω^+ are generated at 4 and 12 eV, respectively. The contribution of the oxide losses ($\hbar\omega > 10$ eV) are slightly reduced, but in comparison with the experimental measurements, they remain too strong. The low-loss peak (ω^-) is predicted to occur at a slightly higher energy (4–5 eV). This fact probably indicates a small difference between the properties of the oxide layer covering the particle and the SiO_2 (glass), assumed for the calculations.

The next step consists in comparing the predicted localization for the different excitations with the experimental measurements. This kind of direct comparison, between calculated probabilities and energy-filtered image intensities, has been criticized by several authors, because the measured profiles may contain effects such as multiple scattering, focusing, etc., not included in the simple dielectric energy-loss probability calculation. Multiple events may be neglected because of the small dimension of the objects under study. We have included, in the calculated profile, an integration window of 1 eV, to take into account the energy width admitted by the selection slits of the spectrometer. The line profile surface losses across the particles at 3.5 and 8.5 eV are shown in Fig. 11. As before, the individual multipoles are in the lower part and the addition of the 12 first multipoles in the upper part. A few immediate conclusions can be made. (a) The energy-loss probability shows some oscillations as a function of the probe position, and the number of these oscillations increases with the index l. (b) The spatial distribution becomes narrower at the interface with increasing l, the first two modes $l = 1$ and 2 are less localized, but most intense. (c) The contribution of the dipole mode is more important for the 9-eV plasmon (di-

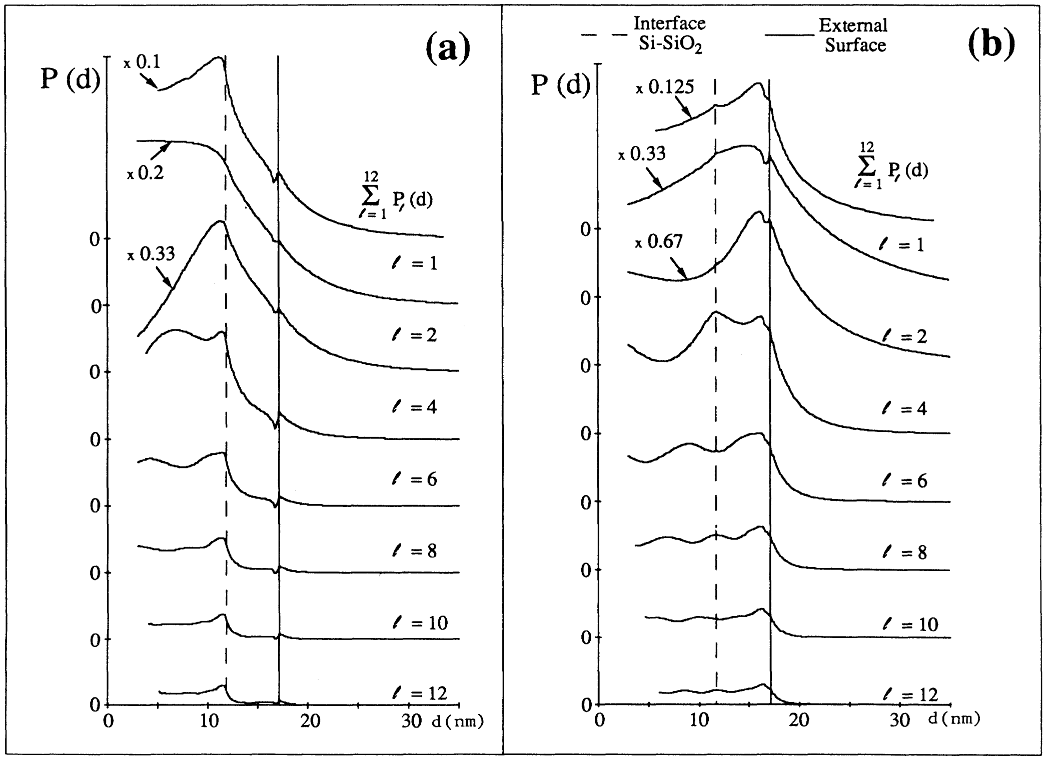

FIG. 11. Calculated surface loss probabilities as a function of impact parameter d for a doubly coated sphere. The intensity is integrated over an energy window of 1 eV full width. (a) 8.5 eV; (b) 3.5 eV.

vided by 5) than for the ω^- mode (divided by 3). (d) The summation of the different multipoles up to $l=12$ shows that the 9-eV loss is localized at the Si-SiO$_2$ interface and is slightly broader than the 3–4 eV profile maximum, localized near the external surface of the particle. The width and positions of these maxima are in good agreement with the experimental profiles in Fig. 4.

Figure 11 also shows rapid variations in intensity for impact parameters corresponding to the conducting layer. They are produced by the Begrenzungeffekt discussed previously, and they vanish when calculating the total energy loss, which includes volume-plasmon losses that show a strong complementary behavior.

For a comprehensive comparison with experimental profiles, the total energy loss, including surface- and volume-plasmon losses that cannot be discriminated in the experiment, has been evaluated for each position of the probe. As suggested by Ritchie and Howie,[32] the spatial distribution of electrons within the probe is simulated by convolution with a Gaussian profile of FWHM 0.94 nm. The result is shown in Fig. 12, which displays the predicted profiles for the simple oxidized Si particle, the doubly coated Si particle, and the experimental intensities. In the first case, no contrast is detectable at the external surface. The 3–4 eV ring at the external surface is the only clear difference between the two models. It is important to emphasize that energy-filtered images at this energy loss constitute the only way of demonstrating its origin as being due to the existence of a conducting surface layer. The intensity predicted at 3–4 eV is weaker than in the experiment, but the zero-loss peak contribution, which is very important in this energy range, has not been taken into account. As for the volume-plasmon excitations, the oxide plasmon profile (23 eV) is too low with respect to the Si loss (17 eV). In contrast, the probabilities calculated for grazing incidence show an overestimation of the surface-oxide losses (Fig. 10). This fact may originate from a difference between the stoichiometric SiO$_2$ glass, assumed to model the silicon oxide, and the real properties of the natural oxide layer.

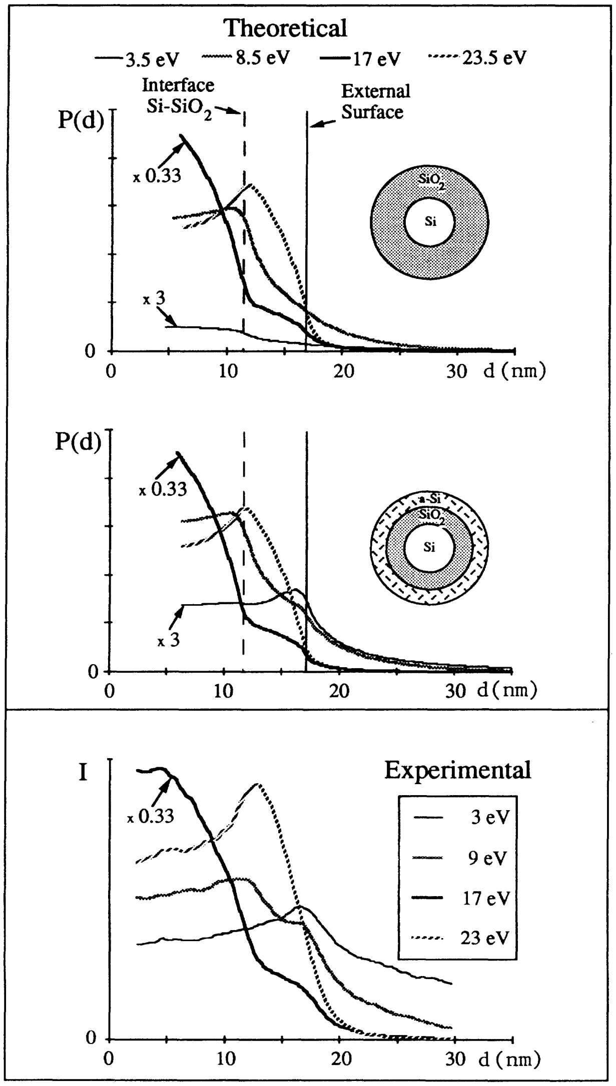

FIG. 12. Comparison between the experimental line profile intensities and the calculated total-energy-loss probability as a function of impact parameter d. The probabilities are obtained using an integration energy window of 1 eV, and a convolution with a Gaussian profile (FWHM 0.94 nm) in order to include the spatial extension of the electron probe.

V. CONCLUSIONS

Classical dielectric theory has been tested on small semiconducting spherical particles. It has been applied to a very complex (doubly coated sphere) and to a heterogeneous situation (inclusion of a 0.5-nm layer). In spite of the simplified description of the sample with abrupt interfaces, dielectric theory is capable of explaining the spatial resolution in energy-filtered images of valence excitations. The expressions developed in this work are valid for an arbitrary dielectric function $\epsilon(\omega)$, and the predictions of the energy-loss probability show a close agreement with the experimental results, even in minor details, provided that the experimental values are used to describe the dielectric permittivity of the material.

We have demonstrated that as the multipole order l grows, the modes are dominated by the surface-oxide losses and contain negligible surface-plasmon contributions. Increasing the value of l also means that the physical properties associated with these multipoles are more and more localized ($q \sim R/l$), giving rise to a transfer from collective excitations to individual excitations. This fact is not included in the classical dielectric theory used here, which neglects the effects of spatial dispersion. Ekardt[44] has shown that for very small alkali-metal particles ($\sim$nm), a limiting l value exists for the conservation of the collective character. Beyond this value, multipoles contain exclusively individual excitations. This fact may explain why the classically calculated energy loss, including high-order multipoles, seems to overestimate the oxide losses. The calculations have been carried up to high-order multipoles ($l=15$) to obtain a correct stability of the results, but high-order multipoles may produce incorrect results in the classical description, and moreover they consume much computer time, so that an optimum $l_{\max}$ value lies generally between 10 and 15.

In the present study, an anomalous result is interpreted by the inclusion of a very thin film (0.5 nm), in the framework of classical dielectric theory, which means that such a thin layer is described as a homogeneous film with the same dielectric properties as the bulk materials. The validity of this approach may be open to question. As many authors have reported the failure of detecting thin coatings or surface reconstructions, with energy-loss experiments using a high-energy electron beam,[45,46] further research work on the sensitivity of low-loss spectroscopic studies to extremely thin surface coatings will be necessary.

ACKNOWLEDGMENTS

The authors thank S. Iijima for providing the specimen for this work and M. Tencé for the invaluable help in manipulation of the STEM digital control.

APPENDIX

To determine the electrostatic potential of the system formed by the impinging electron and the small sphere, we write the solution to the Poisson equation (2a) as

$$\Phi=\Phi_0-\frac{e}{\epsilon(\omega)}\frac{1}{|\mathbf{r}-\mathbf{r}'|}\ ,$$

where Φ_0 is the potential produced by the polarization of the sphere. $\mathbf{r}'$ is the position of the electron.

The potential can be expanded in spherical coordinates (r,θ,φ):

$$\Phi(\mathbf{r},t)=\sum_l \frac{4\pi}{(2l+1)}\sum_{m=0}^{l} P_l^m(\cos\theta)P_l^m(\cos\theta')f_l(r,r')\ ,$$

where

$$f_l(r,r')=\begin{cases} A_l(r/r_1)^l-\dfrac{1}{\epsilon_1}g_l(r,r'), & 0>r>r_1 \\ B_l(r/r_1)^l+C_l(r/r_2)^{-(l+1)}-\dfrac{1}{\epsilon_2}g_l(r,r')\ , & r_1>r>r_2 \\ D_l(r/r_2)^l+E_l(r/R)^{-(l+1)}-\dfrac{1}{\epsilon_3}g_l(r,r'), & r_2>r>R \\ F_l(r/R)^{-(l+1)}-\dfrac{1}{\epsilon_0}g_l(r,r'), & R<r\ , \end{cases}$$

$$g_l(r,r')=\begin{cases} [r^l/(r')^{-(l+1)}], & r'>r \\ [(r')^l/r^{-(l+1)}], & r>r'\ . \end{cases}$$

The coefficients $A_l,\ldots,D_l$ are calculated by solving the following linear system of equations, obtained by applying the usual boundary conditions:

$$\mathcal{M}\cdot\chi=\kappa\ ,$$

where

$$\mathcal{M}=\begin{bmatrix} 1 & -1 & -\alpha^{l+1} & 0 & 0 & 0 \\ 0 & \alpha^l & 1 & -1 & -\gamma^{l+1} & 0 \\ 0 & 0 & 0 & \gamma^l & 1 & -1 \\ \epsilon_1 l & -\epsilon_2 l & \epsilon_2(l+1)\alpha^{l+1} & 0 & 0 & 0 \\ 0 & \epsilon_2 l\alpha^l & -\epsilon_2(l+1) & -\epsilon_3 l & \epsilon_3(l+1)\gamma^{l+1} & 0 \\ 0 & 0 & 0 & \epsilon_3 l\gamma^l & -\epsilon_3(l+1) & \epsilon_0(l+1) \end{bmatrix}\ ,$$

$$\chi=\begin{bmatrix} A_l \\ B_l \\ C_l \\ D_l \\ E_l \\ F_l \end{bmatrix},\quad \kappa=\begin{bmatrix} g_l(r_1,r')\dfrac{\epsilon_2-\epsilon_1}{\epsilon_2\epsilon_1} \\ g_l(r_2,r')\dfrac{\epsilon_3-\epsilon_2}{\epsilon_3\epsilon_2} \\ g_l(R,r')\dfrac{\epsilon_0-\epsilon_3}{\epsilon_0\epsilon_3} \\ 0 \\ 0 \\ 0 \end{bmatrix}\ .$$

The energy-loss probability is then calculated as

$$P_\omega(d)=\frac{e}{2\pi\hbar v^2}\mathrm{Im}[\Phi_0(\mathbf{d},k_z,\omega)|_{k_z=-\omega/v}]\ .$$

To perform the calculation of expression (10) the following coefficients are necessary:

$$\tilde{\chi}^{k}_{l_m}(\omega)=\mathcal{F}(P_l^m(\cos\theta')\chi_l^k)$$

($\mathcal{F}$ denotes Fourier-transform operation),

$$\eta=[\det(\mathcal{M})]^{-1}=[-(\alpha\gamma)^{2l+1}a_{03}a_{32}a_{21}-\alpha^{2l+1}l(l+1)d_{03}d_{32}a_{21}-\gamma^{2l+1}l(l+1)a_{03}d_{23}d_{21}-l(l+1)d_{03}a_{23}d_{21}]^{-1} ,$$

$$x_l^{1,1}=\frac{-(l+1)}{\epsilon_1}\eta[(\alpha\gamma)^{2l+1}a_{03}a_{32}d_{21}+\gamma^{2l+1}la_{03}d_{32}d_{21}+\alpha^{2l+1}l(l+1)d_{03}d_{32}d_{21}+ld_{03}a_{23}d_{21}] ,$$

$$x_l^{1,2}=-(l+1)(2l+1)\alpha^{l+1}\eta(\gamma^{2l+1}a_{03}d_{32}+d_{03}d_{32}l) ,$$

$$x_t^{1,3}=-(\alpha\gamma)^{l+1}\eta d_{03}\epsilon_2(l+1)(2l+1)^2 ,$$

$$x_l^{2,1}=\frac{-l(l+1)}{\epsilon_2}\eta d_{21}(\gamma^{2l+1}a_{03}d_{32}+d_{03}a_{23}) ,$$

$$x_l^{2,2}=\frac{-(l+1)}{\epsilon_2}\eta\alpha^{l+1}d_{32}a_{21}(\gamma^{2l+1}a_{03}+d_{03}l) ,$$

$$x_l^{2,3}=-(\alpha\gamma)^{l+1}\eta d_{03}a_{21}(l+1)(2l+1) ,$$

$$x_t^{3,1}=\frac{l}{\epsilon_2}\alpha^l\eta d_{21}[\gamma^{2l+1}a_{03}a_{32}+d_{03}d_{32}l(l+1)] ,$$

$$x_t^{3,2}=\frac{-1}{\epsilon_2}\eta d_{32}d_{21}l(l+1)(\gamma^{2l+1}a_{03}+d_{03}l) ,$$

$$x_l^{3,3}=-\gamma^{l+1}\eta d_{03}d_{21}l(l+1)(2l+1) ,$$

$$x_l^{4,1}=-\alpha^l\eta d_{03}d_{21}l(l+1)(2l+1) ,$$

$$x_l^{4,2}=\frac{l(l+1)}{\epsilon_3}\eta d_{03}d_{32}[-\alpha^{2l+1}a_{21}+d_{21}(l+1)] ,$$

$$x_l^{4,3}=\frac{-(l+1)}{\epsilon_3}\eta\gamma^{l+1}d_{03}[\alpha^{2l+1}a_{32}a_{21}+d_{32}d_{21}l(l+1)] ,$$

$$x_l^{5,1}=(\alpha\gamma)^l\eta a_{03}d_{21}l(2l+1),$$

$$x_l^{5,2}=\frac{l}{\epsilon_3}\gamma^l\eta a_{03}d_{32}[\alpha^{2l+1}a_{21}-d_{12}(l+1)] ,$$

$$x_l^{5,3}=\frac{l(l+1)}{\epsilon_3}\eta d_{03}(\alpha^{2l+1}d_{32}a_{21}+a_{23}d_{21}) ,$$

$$x_l^{6,1}=(\alpha\gamma)^l\eta\epsilon_3d_{21}l(2l+1)^2 ,$$

$$x_l^{6,2}=\gamma^l\eta d_{32}l(2l+1)[\alpha^{2l+1}a_{21}-d_{21}(l+1)] ,$$

$$x_l^{6,3}=\frac{d_{03}l}{\epsilon_0}\eta[(\alpha\gamma)^{2l+1}a_{32}a_{21}+\gamma^{2l+1}d_{32}d_{21}l(l+1)-\alpha^{2l+1}d_{32}a_{21}(l+1)-a_{23}d_{21}(l+1)] .$$

---

*Present address: Institut de Physique Experimentale, Ecole Polytechnique Fédérale de Lausanne, PHB Ecublens, 1015 Lausanne, Switzerland.

[1] M. Scheinfein, Scanning Microsc. Suppl. **1**, 166 (1987).

[2] F. Fujimoto and K. Komaki, J. Phys. Soc. Jpn. **25**, 1679 (1968).

[3] H. Petersen, Solid State Commun. **23**, 931 (1977).

[4] P. E. Batson, Phys. Rev. Lett. **49**, 936 (1982).

[5] Z. L. Wang and J. M. Crowley, Ultramicroscopy **21**, 77 (1987).

[6] F. Ouyang and M. Isaacson, Ultramicroscopy **31**, 345 (1989).

[7] B. L. Illman, V. E. Anderson, R. J. Warmack, and T. L. Ferrell, Phys. Rev. B **38**, 3045 (1988).

[8] A. Murray, M. Isaacson, and I. Adesida, Appl. Phys. Lett. **45**, 589 (1984).

[9] S. D. Berger, I. G. Salisbury, R. H. Milne, D. Imeson, and C. J. Humphreys, Philos. Mag. B **55**, 341 (1987).

[10] M. Schmeits, Solid State Commun. **67**, 172 (1988).

[11] C. A. Walsh, Philos. Mag. B **59**, 227 (1989).

[12] N. Zabala, A. Rivacoba, and P. M. Echenique, Surf. Sci. **209**, 465 (1989).

[13] M. Schmeits, Phys. Rev. B **39**, 7567 (1989).

[14] P. E. Batson, Ultramicroscopy **9**, 277 (1982).

[15] Z. L. Wang and J. M. Cowley, Ultramicroscopy **21**, 335 (1987).

[16] M. Achèche, C. Colliex, H. Kohl, A. Nourtier, and P. Trebbia, Ultramicroscopy **20**, 99 (1986).

[17] E. D. Palik, in *Handbook of Optical Constants of Solids*, edited

by E. D. Palik (Academic, London, 1985).

[18] C. Mory, Doctorat d'Etat dissertation, Université de Paris, XI, 1985.

[19] S. Iijima, Jpn. J. Appl. Phys. **26**, 357 (1987).

[20] M. Schmeits, J. Phys. C **14**, 1203 (1981).

[21] A. Howie and R. H. Milne, Ultramicroscopy **18**, 427 (1985).

[22] M. Walls and A. Howie, Ultramicroscopy **28**, 40 (1989).

[23] H. Raether, in *Excitations of Plasmons and Interband Transitions by Electrons,* edited by G. Höhler, Springer Tracts in Modern Physics Vol. 88 (Springer-Verlag, New York, 1980).

[24] S. Munnix and M. Schmeits, Phys. Rev. B **32**, 4192 (1985).

[25] D. B. Tran Thoai and E. Zeitler, Appl. Phys. A **45**, 249 (1988).

[26] R. Ruppin, J. Phys. Chem. Solids **39**, 233 (1978).

[27] H. Kohl, Ultramicroscopy **11**, 53 (1983).

[28] T. L. Ferrell and P. M. Echenique, Phys. Rev. Lett. **55**, 1526 (1985).

[29] F. Ouyang and M. Isaacson, in *Proceedings of the 47th Annual Meeting of the Electron Microscopy Society of America, San Antonio, 1989,* edited by G. W. Wailey (San Francisco Press, San Francisco, 1989), p. 230.

[30] A. vom Felde, J. Fink, and W. Ekardt, Phys. Rev. Lett. **61**, 2249 (1988).

[31] A. D. Boardman and B. D. Paranjape, J. Phys. F **7**, 1935 (1977).

[32] R. H. Ritchie and A. Howie, Philos. Mag. A **58**, 753 (1988).

[33] P. M. Echenique, A. Howie, and D. J. Wheatley, Philos. Mag. B **56**, 335 (1987).

[34] J. Baussels, A. Rivacoba, and P. M. Echenique, Surf. Sci. **189/190**, 1015 (1988).

[35] R. Rojas, F. Claro, and R. Fuchs, Phys. Rev. B **37**, 6799 (1988).

[36] R. F. Egerton, *Electron Energy Loss Spectroscopy in the Electron Microscope* (Plenum, New York, 1986).

[37] H. J. Hagemann, W. Gudat, and C. Kunz (unpublished).

[38] M. R. Mc Cartney and D. J. Smith, Surf. Sci. **221**, 214 (1989).

[39] R. H. Ritchie, Phys. Rev. **106**, 874 (1957).

[40] C. Colliex, Ultramicroscopy **18**, 131 (1985).

[41] D. Ugarte, Ph. D. dissertation, Université de Paris XI, Orsay, 1990.

[42] H. Boersch, J. Geiger, and W. Stickel, Z. Phys. **212**, 130 (1968).

[43] M. G. Walls, in *Analytical Electron Microscopy Workshop EMAG'87, Manchester, 1987,* edited by G. W. Lorimer (Institute of Metals, Brookfield, VT, 1987), p. 115.

[44] W. Eckardt, Phys. Rev. B **32**, 1961 (1985).

[45] O. L. Krivanek, Y. Tanishiro, K. Takayanagi, and K. Yagi, Ultramicroscopy **11**, 215 (1983).

[46] A. Howie, in *Surface and Interface Characteristics by Electron Optical Methods,* edited by A. Howie and U. Valdré (Plenum, New York, 1987), p. 19.

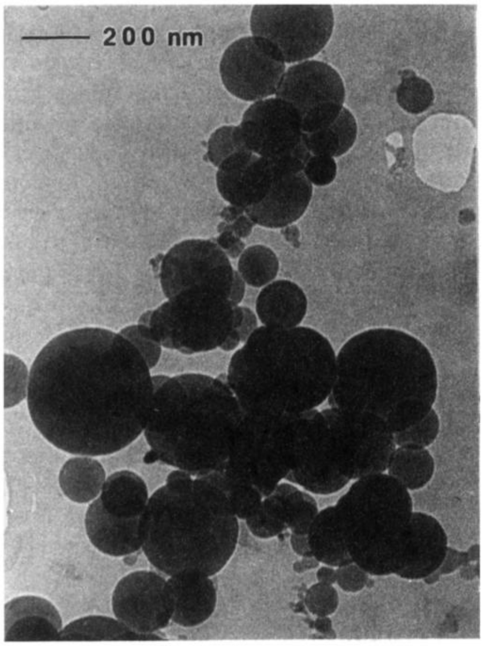

FIG. 1. Conventional electron micrograph of a group of silicon particles.

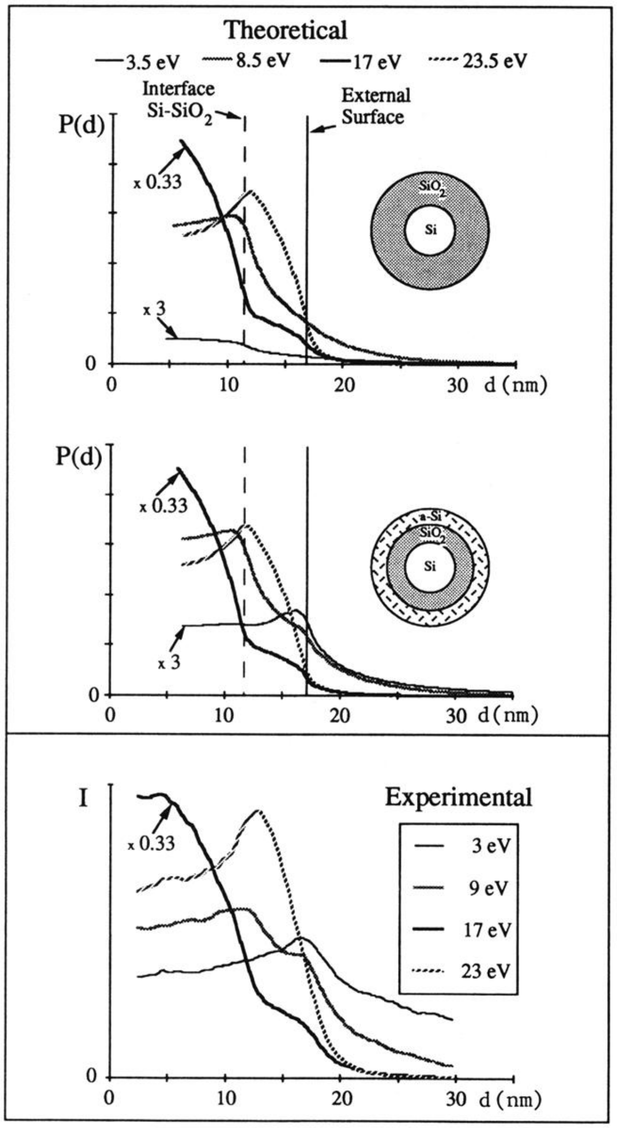

FIG. 12. Comparison between the experimental line profile intensities and the calculated total-energy-loss probability as a function of impact parameter *d*. The probabilities are obtained using an integration energy window of 1 eV, and a convolution with a Gaussian profile (FWHM 0.94 nm) in order to include the spatial extension of the electron probe.

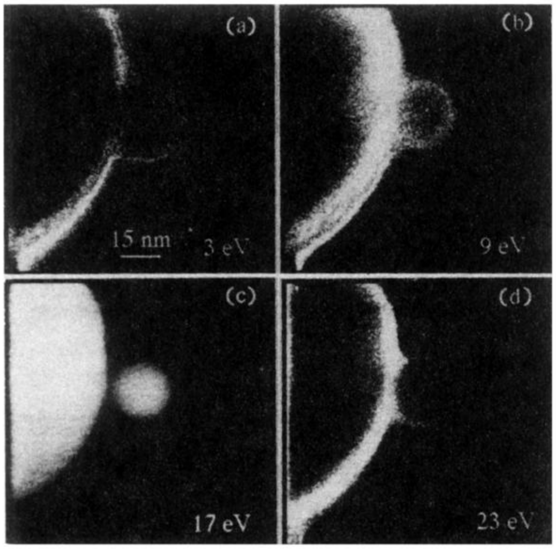

FIG. 3. Series of energy-filtered images of a small silicon particle close to a bigger one.

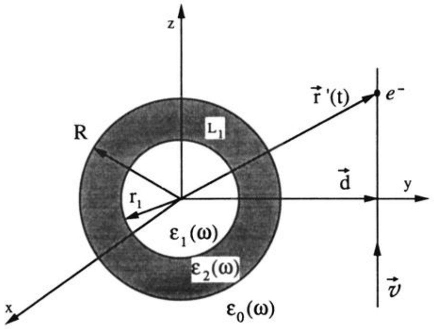

FIG. 5. Electron traveling with a velocity v at an impact parameter d from an oxidized sphere of external radius R.

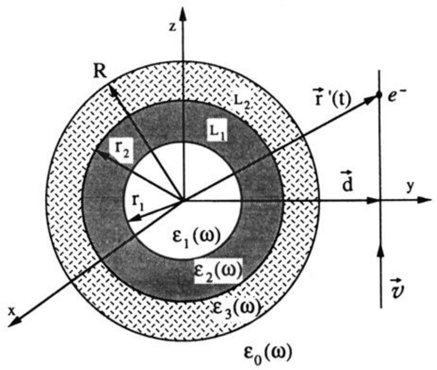

FIG. 8. Electron traveling with a velocity v at an impact parameter d from a doubly coated sphere of external radius R.